

# SilhoNet: An RGB Method for 3D Object Pose Estimation and Grasp Planning

Gideon Billings<sup>1</sup> and Matthew Johnson-Roberson<sup>1</sup>

**Abstract**— Autonomous robot manipulation often involves both estimating the pose of the object to be manipulated and selecting a viable grasp point. Methods using RGB-D data have shown great success in solving these problems. However, there are situations where cost constraints or the working environment may limit the use of RGB-D sensors. When limited to monocular camera data only, both the problem of object pose estimation and of grasp point selection are very challenging. In the past, research has focused on solving these problems separately. In this work, we introduce a novel method called SilhoNet that bridges the gap between these two tasks. We use a Convolutional Neural Network (CNN) pipeline that takes in region of interest (ROI) proposals to simultaneously predict an intermediate silhouette representation for objects with an associated occlusion mask. The 3D pose is then regressed from the predicted silhouettes. Grasp points from a precomputed database are filtered by back-projecting them onto the occlusion mask to find which points are visible in the scene. We show that our method achieves better overall performance than the state-of-the-art PoseCNN network for 3D pose estimation on the YCB-video dataset.

## I. INTRODUCTION

Robots are revolutionizing the way technology enhances our lives. From helping people with disabilities perform various tasks around their house to autonomously collecting data in humanly inaccessible environments, robots are being applied across a spectrum of exciting and impactful domains. Many of these applications require the robot to grasp and manipulate an object in some way (e.g., opening a door by a handle, or picking up an object from the seafloor), but this poses a challenging problem. Specifically, the robot must interpret sensory information of the scene to both localize the object and plan a grasp approach. One method to solve this problem is to identify an object and determine its pose relative to the robot [1]. Using this information, precomputed grasp points can be retrieved and manipulation can be planned. While previous methods that use this approach generally relied on depth information of the scene, one remaining open challenge is determining in real-time which of these precomputed grasp points are accessible based on monocular camera data only. Moreover, when the sensor modality is limited to monocular images, estimating the pose of an object and determining a good grasp point in a natural setting are challenging problems due to variability in scene illumination, the variety of object shapes and textures, and occlusions caused by scene clutter.

Previous methods for object pose estimation and grasping largely depend on RGB-D data about the 3D working environment [1]–[4]. However, there are cases where such depth information is not readily available. Some examples include systems that operate outdoors where common depth sensors like the Kinect do not work well, embedded systems where space and cost may limit the size and number of sensors, and underwater vehicles where the variable and scattering properties of the water column result in noisy and sparse depth information. In these scenarios, methods that operate on monocular camera data are needed.

Recently, there has been great progress in state-of-the-art methods for monocular image pose estimation on difficult datasets, where the scenes are cluttered and objects are often heavily occluded [5]–[11]. Also, there has been recent work on learning methods for grasp point prediction that operate in RGB [12], [13]. While these methods solve the problem of either pose estimation or grasp point prediction in RGB, there is little work bridging the gap between the two problems.

One of the key ideas motivating this work is that occlusion information about an object from a monocular camera viewpoint can be used to filter candidate grasp points computed offline from high resolution 3D models [1]. This filtering can be used to determine if the object is free enough of surrounding clutter to attempt a grasp. Choosing a visually unoccluded grasp point is relevant for tasks where the manipulator could be damaged by jamming into an unexpected barrier, such as when operating in disaster response sites or commercial plants, or where the manipulator itself may cause unwanted damage to its surroundings, such as when operating in fragile underwater habitats.

In this paper, we present the following contributions: 1) SilhoNet, a novel RGB-based deep learning method to estimate pose and occlusion in cluttered scenes; 2) The use of an intermediate silhouette representation to facilitate learning a model on synthetic data to predict 3D object pose on real data, effectively bridging the sim-to-real domain shift [14]; 3) A method to select unoccluded grasp points, using the projection of inferred silhouettes, in novel scenes; 4) An evaluation on the visually challenging YCB-Video dataset [7] where the proposed approach outperforms a state-of-the-art RGB method [7].

The rest of this paper is organized in the following sections: section II discusses related work; section III presents our method with an overview of our CNN design for 3D pose estimation and occlusion mask prediction, along with the technique used to filter potential grasp points based on the occlusion mask; section IV presents the experimental results;

<sup>1</sup>Gideon Billings and Matthew Johnson-Roberson are with DROP lab, Department of Naval Architecture and Marine Engineering, University of Michigan, Ann Arbor, MI 48109, USA [gidobot@umich.edu](mailto:gidobot@umich.edu), [mattjr@umich.edu](mailto:mattjr@umich.edu)

and section V concludes the paper.

## II. RELATED WORK

In the following sections, we present a brief overview of the most relevant existing work for object pose estimation and grasp point prediction.

### A. Pose Estimation

Extensive research has focused on 6D object pose estimation using RGB-D data. Several works rely on feature- and shape-based template matching to locate the object in the image and coarsely estimate the pose [5], [15], [16]. This is often followed by a refinement step using the Iterative Closest Point (ICP) algorithm with the 3D object model and a depth map of the scene [15]. While these methods are computationally efficient, their performance often degrades in cluttered environments. Other methods have exploited point cloud data to match 3D features and fit the object models into the scene [17], [18]. While point cloud based methods achieve state-of-the-art performance, they can be very computationally expensive. Recent works have demonstrated the power of machine learning for object detection and pose estimation using RGB-D data. Schwarz *et al.* [19] used a CNN pretrained on ImageNet to extract features from an RGB image and a colorized depth map. They learned a series of Support Vector Machines (SVM) on top of these extracted features to predict the object category and a single axis rotation about a planar surface normal. In [20], they trained a decision forest to regress every pixel from an RGB-D image to an object class and a coordinate position on the object model. Other work has used a CNN to map the pose of an object in an observed RGB-D image to a rendered pose of the model through an energy function [21]. The minimization of the energy function gives the object pose. Michel *et al.* [22] trained a Conditional Random Field (CRF) to output a number of pose-hypotheses from a dense pixel wise object coordinate prediction map computed by a random forest. A variant of ICP was used to derive the final pose estimate. While these learning-based methods are powerful, efficient, and give state-of-the-art results, they rely on RGB-D data to estimate the object pose.

There are several recent works extending deep learning methods to the problem of 6D object pose estimation using RGB data only. Rad *et al.* [6] and Tekin *et al.* [8] used a CNN to predict 2D projections of the 3D object bounding box corners in the image, followed by a PnP algorithm to find the correspondences between the 2D and 3D coordinates and compute the object pose. Xiang *et al.* [7] proposed a multistage, multibranch network with a Hugh Voting scheme to directly regress the 6D object pose as a 3D translation and a unit quaternion orientation. Kehl *et al.* [9] predicted 2D bounding box detections with a pool of candidate 6D poses for each box. After a pose refinement step, they choose the best candidate pose for each box. Li *et al.* [10] used an end-to-end CNN framework to predict discretely binned rotation and translation values with corrective delta offsets. They proposed a novel method for infusing the class prior

into the learning process to improve the network performance for multi-class prediction. Li *et al.* [11] proposed a deep-learning-based iterative matching algorithm for RGB based pose refinement, which achieves performance close to methods that use depth information with ICP. These RGB-based pose estimation methods demonstrate competitive performance against state-of-the-art approaches that rely on depth data. However, beyond providing the estimated pose, these methods provide little information about the context of the cluttered scene around the object for effective grasp planning.

### B. Grasping

Methods for grasp planning can be classified into two general categories: analytic and data-driven approaches [1]. Analytic approaches are sensitive to random and systematic errors found in real robot systems, so recent methods have focused on the data-driven approach, which can be further divided into two broad strategies. In the first strategy, information about the detected object and the estimated pose are used to filter potential grasp points or previous grasp experiences from a precomputed database [1]. In the second strategy, the grasp approach is learned in an end-to-end framework where the grasp point is synthesized on the fly [12], [13], [23]. In our work, we focus on the data-driven approach to grasp prediction for known objects using a precomputed grasp point database.

Early work on the data-driven approach to grasping relied on feature matching with RANSAC to detect known objects in stereo data and fit a 3D model into the scene [24]–[26]. Some methods operate on point cloud data to register known 3D models into the scene [27], [28]. While these feature-based approaches have been shown to work effectively in cluttered environments, they depend on object texture or color blob information to match the known model features, and they suffer in variable lighting conditions or when dealing with textureless objects. Our method is designed to be robust for both textured and textureless objects and handle variable lighting conditions.

More recently, there has been work to leverage the power of deep learning for grasp prediction. Lenz *et al.* [29] introduced a cascaded CNN architecture for detecting and filtering grasp candidates in an RGB-D view. This method bypasses the pose estimation step in previous approaches and directly regresses viable grasp points. Additional work has extended the end-to-end approach to difficult datasets with cluttered scenes and demonstrated state-of-the-art performance on pick-and-place challenges [12], [13]. However, by operating in an end-to-end manner, these methods do not provide a pose estimate of the object, which is often desirable for manipulation tasks other than pick-and-place, such as operating a tool where the object must be manipulated in a specific way. There are also many objects in real life that are heterogeneous in construction, and considering the object's weight distribution is important when selecting a grasp point. Prior knowledge of the object with an estimate of the object pose in the scene would provide the information needed to choose good grasp approaches for such objects.

Our method combines the power of deep learning for 3D pose prediction in monocular images with prior knowledge of the object model, and it filters precomputed grasp points by taking into account occlusions from other objects in cluttered environments. Information about how the object is occluded can provide useful insight about the viability of potential grasps, given situations where an unobstructed grasp approach is desirable. Our method effectively bridges the gap between pose estimation and grasp point prediction in cluttered environments, especially when knowledge of the scene is limited to RGB data.

### III. METHOD

We introduce a novel method that operates on monocular color images to estimate the 3D object rotational pose, relative to the camera center, and predict visually unoccluded grasp points. The method operates in two stages, first predicting an intermediate silhouette representation and occlusion mask of an object and then regressing the 3D orientation quaternion from the predicted silhouette. Viable grasp points are determined from a precomputed database of grasps, based on the estimated occlusion of the detected objects in the RGB viewpoint and a priori knowledge of the object models. The following sections describe our method in detail.

#### A. Overview of the Network Pipeline

Figure 1 presents an overview of the network pipeline. The input to the network is an RGB image with bounding box ROI proposals for detected objects and the associated class labels. The first stage uses a VGG16 [30] backbone with deconvolutional layers at the end to produce a feature map from the RGB input image. This feature extraction network is the same as used in PoseCNN [7]. Extracted features from the input image are concatenated with features from a set of rendered object viewpoints and then passed through two network branches of identical structure to predict a full unoccluded silhouette and occlusion mask. The second stage of the network passes the predicted silhouette through a ResNet-18 [31] architecture with two fully connected layers at the end to output an L2-normalized quaternion, representing the 3D pose.

1) *Predicted ROIs*: We trained an off-the-shelf Faster-RCNN implementation from Tensorpack [32] on the YCB-video dataset [7] to predict ROI proposals. The network was trained across two Titan V GPUs for 3,180,000 iterations on the training image set with the default parameters and without any synthetic data augmentation. The ROI proposals are provided as input to the network after the feature extraction stage, where they are used to crop the corresponding region out of the input image feature map. The cropped feature map is then resized to a width and height of 64x64 by either scaling down the feature map or using bi-linear interpolation to scale it up.

2) *Rendered Model Viewpoints*: We were able to boost the silhouette prediction performance by generating a set of synthetic pre-rendered viewpoints associated with the detected object class as an additional input to the first stage

of the network. For each class, we rendered a set of 12 viewpoints from the object model, each with dimension 224x224. These viewpoints were generated using Phong shading at azimuth intervals from 0° to 300° with elevation angles of -30° and 30°. As the intermediate goal is silhouette prediction, these synthetic renders do an excellent job of capturing the shape and silhouette of real objects, in different orientations, despite the typical domain shift in the visual appearance of simulated objects [14].

All the viewpoints for the detected object class are passed through the feature extraction stage and then resized to 64x64 with channel dimension 32 by passing them through a max-pooling layer with width 4 and stride 4, followed by two deconvolutional layers that each increase the feature map size by 4. In our implementation, we extracted the feature maps of the rendered viewpoints on-the-fly for each object detection. However, to increase network performance time, these extracted feature maps can be precomputed and stored offline. These rendered viewpoint feature maps were provided to the network by stacking them on the channel dimension and then concatenating with the cropped and resized input image feature map (Fig.1).

3) *Silhouette Prediction*: The first stage of the network predicts an intermediate silhouette representation of the object as a 64x64 dimensional binary mask. This silhouette represents the full unoccluded visual hull of the object as though it were rendered with the same 3D orientation but centered in the frame. The size of the silhouette in the frame is invariant to the scale of the object in the image and is determined by a fixed distance of the object from the camera at which the silhouette appears to be rendered. This distance is chosen for each object so that the silhouette just fits within the frame for any 3D orientation. This stage of the network also has a parallel branch that outputs a similar silhouette, with only the unoccluded parts of the object visible. We refer to this occluded output as the ‘occlusion mask’.

The first part of the network is a VGG16 feature extractor [30], which generates feature maps at 1/2, 1/4, 1/8, and 1/16 scale. The 1/8 and 1/16 scale feature maps both have an output channel dimension of 512. The channel dimension for both is reduced to 64 using two convolutional layers, after which the 1/16 scale map is upsampled by a factor of 2 using deconvolution and then summed with the 1/8 scale map. The summed map is upsampled by a factor of 8 using a second deconvolution to get a final feature map of the same dimension as the input image with a feature channel width of 64 (Fig.1).

After the input image is passed through the feature extractor, the input ROI proposal for the detected object is used to crop out the corresponding area of the resulting feature map and resize it to 64x64. This feature map is concatenated with the rendered viewpoint feature maps, resulting in a single feature vector matrix with size 64x64x448.

The feature vector matrix is fed into two identical network branches, one of which outputs the silhouette prediction and the other outputs the occlusion mask. Each branch is composed of 4 convolutional layers, each with a filter width,

## Silhouette Prediction

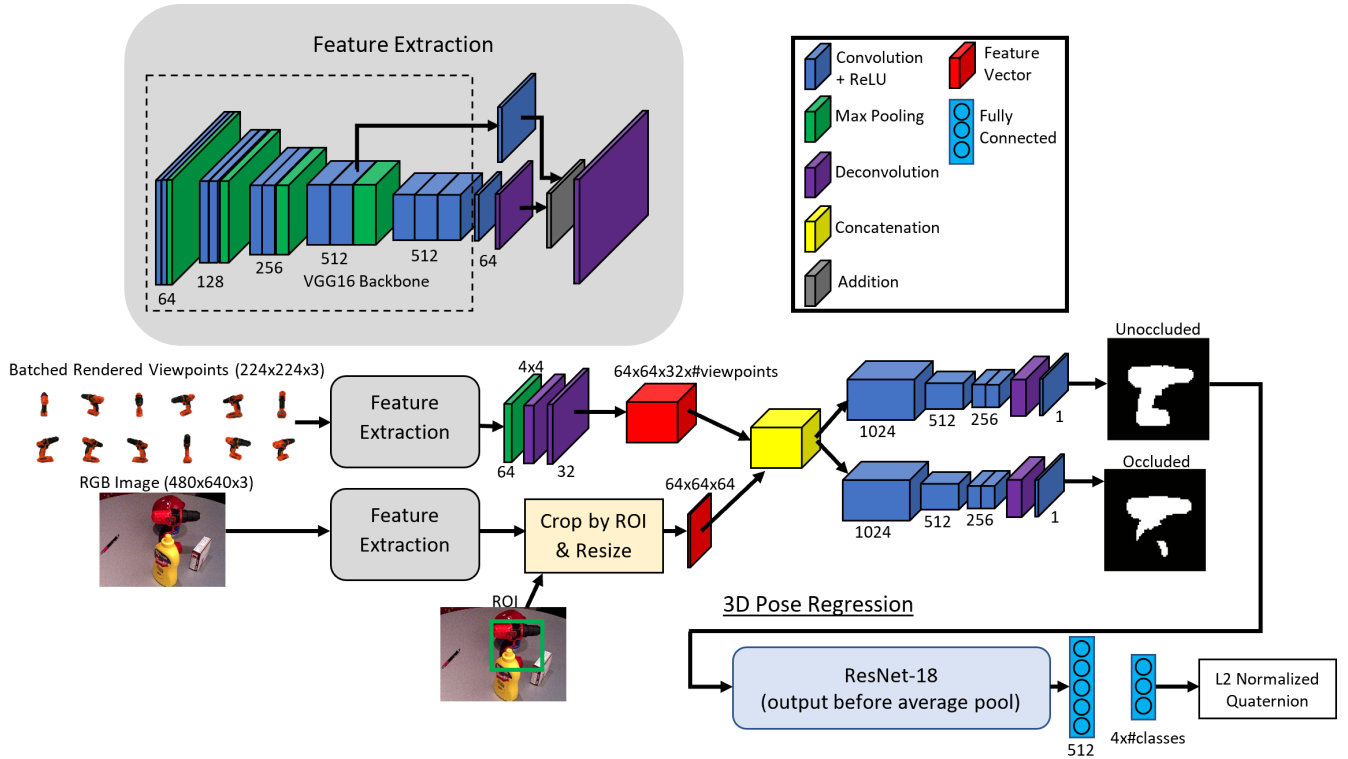


Fig. 1. Overview of the SilhoNet pipeline for silhouette prediction and 3D pose regression

channel dimension, and stride of (2, 1024, 1), (2, 512, 2), (3, 256, 1), and (3, 256, 1) respectively, followed by a deconvolutional layer with filter width, channel dimension, and stride of (2, 256, 2). The output of the deconvolutional layer is fed into a dimension reducing convolutional filter with a single channel output shape of 64x64. A sigmoid activation function is applied at the output to produce a probability map.

4) *3D Pose Regression*: We use a quaternion representation for the 3D pose, which can represent arbitrary 3D rotations in continuous space as a unit vector of length 4. The quaternion representation is especially attractive, as it does not suffer from gimbal lock like the Euler angle representation.

The second stage of the network takes in the predicted silhouette probability maps, thresholded at some value into binary masks, and outputs a quaternion prediction for the object pose. This stage of the network is composed of a ResNet-18 [31] backbone, with the layers from the average pooling and below replaced with two fully connected layers. The last fully connected layer has output dimension  $4 \times (\# \text{ classes})$ , where each class has a separate output vector. The predicted vector for the class of the detected object is extracted from the output and normalized using an L2-norm to get the final quaternion prediction (Fig.1).

Because the silhouette representation of objects is featureless, this method treats symmetries in object shape as equivalent symmetries in the 3D pose space. In many robotic manipulation scenarios, this is a valid assumption. For exam-

ple, a tool such as a screwdriver that may not be symmetric in RGB feature space is symmetric in shape and equivalently symmetric in grasp space. However, it is a future goal of this work to extend the 3D pose estimation to account for non-symmetries in feature space. An example of an object that may be symmetric in shape but not in feature space is a soup can with a feature rich label. In certain manipulation tasks, it may be desirable to orient the label a specific way, in which case, the unique pose in feature space is needed.

By regressing the 3D pose from an intermediate silhouette representation, we were able to train this stage of the network using only synthetically rendered silhouette data. In our results, we show that the network generalized well to predicting pose on real data, showing that this intermediate representation as an effective way to bridge the domain shift between real and synthetic data.

### B. Grasp Point Detection

The final step of our method is detecting visually viable grasp points. Given the estimated 3D pose of the object and a database of precomputed grasp points, we project each grasp point from the object frame onto the occlusion mask in the camera frame. The points that lie on the unoccluded portion of the mask are considered valid, and the highest scoring grasp can be selected from the valid set. We demonstrate our method in figure 4 with a custom generated database of grasp points for the pitcher object. There are many libraries available for facilitating the automatic computation of grasp point databases, such as the DexNet API [33].

### C. Dataset

We evaluated our method on the YCB-video dataset [7], which consists of 92 video sequences composed of 133,827 frames, containing a total of 21 objects, appearing in different arrangements with varying levels of occlusion. Twelve of the video sequences were withheld from the training set for validation and testing. In the silhouette space, the objects in this dataset are characterized by five different types of symmetry: non-symmetric, symmetric about a plane, symmetric about two perpendicular planes, symmetric about an axis, symmetric about an axis and a plane. We applied a rotation correction to the coordinate frame of all objects that exhibit any form of symmetry so that each axis or plane of symmetry aligns with a coordinate axis. Ground truth quaternions were generated from the labeled object poses such that only one unique quaternion is associated with every viewpoint that produces the same visual hull. Having a consistent quaternion label for all matching silhouette viewpoints enabled the pose prediction network to be trained effectively for all types of object symmetries using a very simple distance loss function.

Supplementing the real image data in the YCB-video dataset are 80,000 synthetically rendered images, with all of the 21 objects appearing in various combinations and random poses over a transparent background. We supplement the training data by randomly sampling images from the COCO-2017 dataset [34] and applying them as background to these synthetic images at training time.

### D. Network Training

All networks were trained with the Adam optimizer on either a Titan V or Titan X GPU. The VGG16 backbone was initialized with ImageNet pre-trained weights, and the silhouette prediction network was trained using cross entropy loss with a batch size of 6 for 325,000 iterations. We trained the network with ground truth ROIs and tested against both ground truth ROIs and predicted ROIs from a Faster-RCNN network [32] trained on the YCB-video dataset.

The 3D pose regression network was trained using the following log distance function between the predicted and ground truth quaternions

$$QLoss(\tilde{q}, q) = \log(\epsilon + 1 - |\tilde{q} \cdot q|), \quad (1)$$

where  $q$  is the ground truth quaternion,  $\tilde{q}$  is the predicted quaternion, and  $\epsilon$  is a small value for stability, in our case  $e^{-4}$ . The pose prediction network was trained for 380,000 iterations with a batch size of 16, using only perfect ground truth silhouettes for training. Testing was done on the predicted silhouettes from the first stage network.

To reduce overfitting during training of the silhouette prediction network, dropout was applied at a rate of 0.5 before the last deconvolution layer of the feature extraction network and on the fourth convolutional layer of each silhouette prediction branch. During training of the 3D pose regression network, dropout was applied at a rate of 0.8 before the first fully connected layer. As a further strategy to reduce overfitting and extend the training data, the hue, saturation,

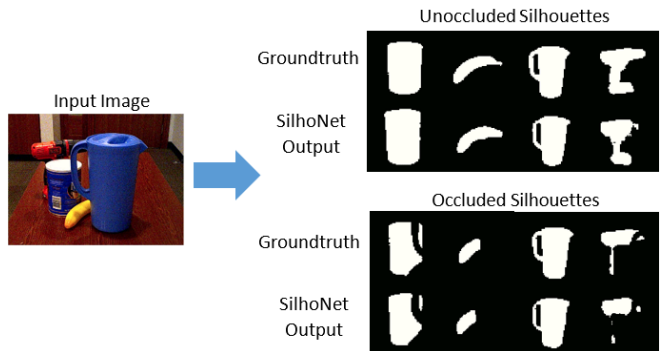


Fig. 2. Example prediction of occluded and unoccluded silhouettes from a test image

and exposure of the training images were randomly scaled by a factor of up to 1.5.

## IV. RESULTS

The following sections present the performance of SilhoNet, tested on the YCB-video dataset [35]. Section A presents the accuracy of the silhouette prediction stage. Section B compares the 3D pose estimation performance of SilhoNet against the performance of PoseCNN. And section C discusses the method for grasp point detection using the predicted occlusion mask and 3D pose.

### A. Silhouette Prediction

We tested the performance of the silhouette prediction stage of SilhoNet with both ground truth ROI inputs from the YCB dataset and predicted ROI inputs from the FasterRCNN network. Figure 2 shows an example of the silhouette predictions for one of the images in the test set. Table I presents the accuracy for the occluded and unoccluded silhouette predictions, measured as the mean intersection over union (IoU) of the predicted silhouettes with the ground truth silhouettes. Overall, the performance degrades a few percent when the predicted ROIs are provided as input rather than the ground truth, but across most classes, the predictions are robust to the ROI input. The largest degradations in performance when using the predicted ROIs are for the "037\_scissors" and "011\_banana" classes, which have thin and low-texture features.

### B. 3D Pose Regression

We compare the performance of the 3D pose predictions from SilhoNet against the published results of PoseCNN, both with and without Iterative Closest Point (ICP) refinement. Figure 3 shows the accuracy curves for both methods of PoseCNN and SilhoNet with YCB ground truth ROI input and FasterRCNN predicted ROI input. The overall performance of SilhoNet is comparable for both ground truth and predicted ROIs, and overall, SilhoNet significantly outperforms PoseCNN with and without ICP refinement. Table II presents the mean accuracy errors for each class across both the PoseCNN and SilhoNet methods. The class with the worst prediction accuracy for SilhoNet relative to PoseCNN is "021\_bleach\_cleanser". SilhoNet treats this object as non-symmetric in silhouette space, but the shape is nearly planar symmetric, so pose predictions from silhouettes

TABLE I

MEAN IOU ACCURACY FOR PREDICTED SILHOUETTES ON THE YCB-VIDEO TEST SET. YCB COLUMNS SPECIFY GROUND TRUTH ROI INPUT, FASTERRCNN COLUMNS SPECIFY PREDICTED ROI INPUT

Object	Unoccluded YCB	Occluded YCB	Unoccluded FasterRCNN	Occluded FasterRCNN
002_master_chef_can	96.73	89.64	96.96	87.74
003_cracker_box	93.25	83.13	89.02	68.75
004_sugar_box	94.57	90.87	92.52	89.24
005_tomato_soup_can	96.85	94.41	96.58	93.46
006_mustard_bottle	95.16	94.18	94.69	94.29
007_tuna_fish_can	96.01	93.54	95.00	93.20
008_pudding_box	94.12	86.71	91.32	76.96
009_gelatin_box	94.64	93.65	93.18	92.85
010_potted_meat_can	93.09	86.57	93.36	87.16
011_banana	87.16	87.47	78.95	77.44
019_pitcher_base	94.93	93.69	92.34	91.90
021_bleach_cleanser	92.95	90.62	91.76	87.40
024_bowl	82.48	76.84	84.62	75.96
025_mug	94.61	86.68	90.72	82.97
035_power_drill	89.51	87.37	77.91	74.12
036_wood_block	87.49	74.99	86.10	76.41
037_scissors	58.73	68.79	49.75	58.27
040_large_marker	83.63	82.72	86.19	84.64
051_large_clamp	84.98	81.04	81.75	78.78
052_extra_large_clamp	84.63	82.05	73.63	68.86
061_foam_brick	90.96	81.63	90.11	70.43
ALL	89.83	86.03	86.97	81.47

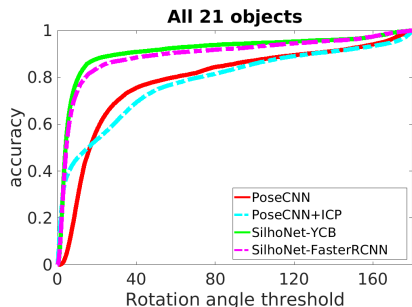


Fig. 3. 3D pose accuracy curve across all objects in the YCB-video dataset. Accuracy is percentage of angle errors less than the rotation angle threshold.

may be easily confused. SilhoNet outperforms PoseCNN by a large margin for several objects that have low texture. The best example of this is the "011\_banana" class, which is non-symmetric in both feature and silhouette space.

### C. Grasp Point Detection

A goal of this method is to fuse 3D pose estimation of objects in monocular images with unoccluded grasp point detection for grasp planning in cluttered scenes. We accomplish this by taking precomputed grasp points in the object frame and projecting them onto the predicted object occlusion mask. Those points that do not lie on the occlusion mask are considered invalid. Figure 4 presents a schematic overview of the process for combining predicted occlusion masks and 3D pose estimates with a precomputed grasp database to filter visible grasp points. The final image in the diagram shows the grasp points projected back into the scene and colored by which points are visible and therefore valid. Understanding which grasp points are occluded can enable the robot to determine if the object is clear enough to make the grasp or if some other step must be taken to enable unobstructed grasping of the object.

TABLE II

MEAN 3D POSE ROTATION ERROR IN DEGREES ON THE YCB-VIDEO TEST SET. YCB COLUMNS SPECIFY GROUND TRUTH ROI INPUT, FASTERRCNN COLUMNS SPECIFY PREDICTED ROI INPUT

Object	PoseCNN	PoseCNN+ICP	SilhoNet-YCB	SilhoNet-FasterRCNN
002_master_chef_can	55.3031	69.5578	2.99	<b>2.1</b>
003_cracker_box	14.2408	<b>8.4497</b>	26.7	38.1
004_sugar_box	8.9476	<b>2.1999</b>	16.8	15.5
005_tomato_soup_can	19.3115	34.2128	3.1	<b>3.0</b>
006_mustard_bottle	9.7764	<b>1.9663</b>	5.1	6.0
007_tuna_fish_can	68.6118	77.9807	<b>2.2</b>	<b>2.2</b>
008_pudding_box	5.6653	<b>5.2264</b>	17.0	28.4
009_gelatin_box	12.3332	<b>1.0268</b>	15.1	23.7
010_potted_meat_can	35.1567	29.8377	10.9	<b>6.0</b>
011_banana	66.6038	62.2553	<b>4.5</b>	18.7
019_pitcher_base	16.8581	<b>7.1445</b>	8.7	8.9
021_bleach_cleanser	26.1065	<b>16.5896</b>	54.8	55.7
024_bowl	<b>29.7020</b>	30.0809	32.8	34.7
025_mug	29.7257	41.6253	<b>6.9</b>	18.7
035_power_drill	14.7973	<b>6.9902</b>	9.6	25.9
036_wood_block	105.7854	101.5361	44.6	<b>35.9</b>
037_scissors	163.4286	174.1417	<b>137.5</b>	151.0
040_large_marker	97.3564	94.8869	<b>14.8</b>	15.1
051_large_clamp	43.9701	47.9920	3.9	<b>3.2</b>
052_extra_large_clamp	74.3115	82.6778	<b>8.8</b>	41.8
061_foam_brick	48.6683	46.3223	<b>23.2</b>	24.7
ALL	38.1464	38.9929	<b>15.8</b>	18.8

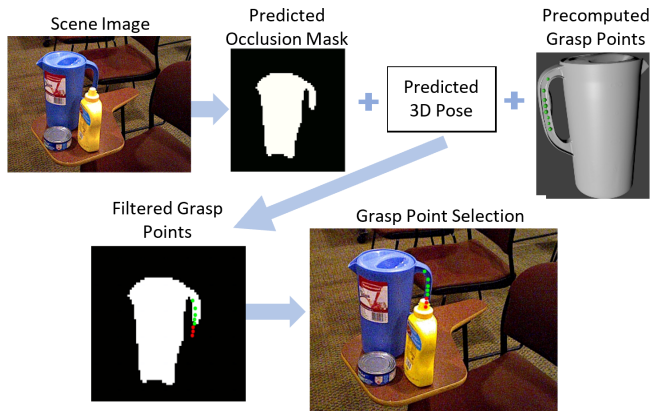


Fig. 4. The occlusion mask is projected onto object model using the predicted 3D pose, and visible grasp points are filtered from a precomputed database. Unoccluded grasp points are shown in green, while occluded points are shown in red.

## V. CONCLUSION

In this paper, we presented a method for object 3D pose estimation from monocular camera images, where detected object ROI proposals are provided as input. We show that this method outperforms the state-of-the-art PoseCNN network for 3D pose estimation across the majority of object classes in the YCB-video dataset. Also, by using an intermediate silhouette representation for detected objects, we show that visually unoccluded grasp points can be detected in the image and used to inform grasp planning from a pre-computed grasp database. Currently, the method predicts 3D poses that are unique to symmetries in silhouette space. Future work will focus on extending this method to pose predictions that are also unique in feature space, despite symmetries in object shape. Also, future work will seek to extend this method to full 6D object pose estimation, towards a full loop object detection and grasp execution pipeline.

## REFERENCES

- [1] J. Bohg, A. Morales, T. Asfour, and D. Kragic, "Data-driven grasp synthesis survey," *IEEE Transactions on Robotics*, vol. 30, no. 2, pp. 289–309, Apr. 2014.
- [2] C. Papazov, S. Haddadin, S. Parusel, K. Krieger, and D. Burschka, "Rigid 3d geometry matching for grasping of known objects in cluttered scenes," *The International Journal of Robotics Research*, vol. 31, no. 4, pp. 538–553, Apr. 2012.
- [3] W. Miyazaki and J. Miura, "Object placement estimation with occlusions and planning of robotic handling strategies," in *2017 IEEE International Conference on Advanced Intelligent Mechatronics (AIM)*, Jul. 2017, pp. 602–607.
- [4] V. Azizi, A. Kimmel, K. Bekris, and M. Kapadia, "Geometric reachability analysis for grasp planning in cluttered scenes for varying end-effectors," in *2017 13th IEEE Conference on Automation Science and Engineering (CASE)*, Aug. 2017, pp. 764–769.
- [5] Z. Cao, Y. Sheikh, and N. K. Banerjee, "Real-time scalable 6dof pose estimation for textureless objects," in *2016 IEEE International Conference on Robotics and Automation (ICRA)*, May 2016, pp. 2441–2448.
- [6] M. Rad and V. Lepetit, "BB8: A scalable, accurate, robust to partial occlusion method for predicting the 3d poses of challenging objects without using depth," *ARXIV:1703.10896 [cs]*, Mar. 31, 2017.
- [7] Y. Xiang, T. Schmidt, V. Narayanan, and D. Fox, "PoseCNN: A convolutional neural network for 6d object pose estimation in cluttered scenes," *ARXIV:1711.00199 [cs]*, Nov. 1, 2017.
- [8] B. Tekin, S. N. Sinha, and P. Fua, "Real-time seamless single shot 6d object pose prediction," *ARXIV:1711.08848 [cs]*, Nov. 23, 2017.
- [9] W. Kehl, F. Manhardt, F. Tombari, S. Ilic, and N. Navab, "SSD-6d: Making RGB-based 3d detection and 6d pose estimation great again," *ARXIV:1711.10006 [cs]*, Nov. 27, 2017.
- [10] C. Li, J. Bai, and G. D. Hager, "A unified framework for multi-view multi-class object pose estimation," *ARXIV:1803.08103 [cs]*, Mar. 21, 2018.
- [11] Y. Li, G. Wang, X. Ji, Y. Xiang, and D. Fox, "DeepIM: Deep iterative matching for 6d pose estimation," *ARXIV:1804.00175 [cs]*, Mar. 31, 2018.
- [12] L. Pinto and A. Gupta, "Supersizing self-supervision: Learning to grasp from 50k tries and 700 robot hours," in *2016 IEEE International Conference on Robotics and Automation (ICRA)*, May 2016, pp. 3406–3413.
- [13] S. Levine, P. Pastor, A. Krizhevsky, J. Ibarz, and D. Quillen, "Learning hand-eye coordination for robotic grasping with deep learning and large-scale data collection," *The International Journal of Robotics Research*, vol. 37, no. 4, pp. 421–436, Apr. 1, 2018.
- [14] A. Carlson, K. A. Skinner, R. Vasudevan, and M. Johnson-Roberson, "Modeling Camera Effects to Improve Deep Vision for Real and Synthetic Data," *ArXiv e-prints*, Mar. 2018.
- [15] S. Hinterstoisser, V. Lepetit, S. Ilic, S. Holzer, G. Bradski, K. Konolige, and N. Navab, "Model Based Training, Detection and Pose Estimation of Texture-Less 3d Objects in Heavily Cluttered Scenes," in *Computer Vision ACCV 2012*, K. M. Lee, Y. Matsushita, J. M. Rehg, and Z. Hu, Eds., Berlin, Heidelberg: Springer Berlin Heidelberg, 2013, pp. 548–562.
- [16] R. Rios-Cabrera and T. Tuytelaars, "Discriminatively trained templates for 3d object detection: A real time scalable approach," in *2013 IEEE International Conference on Computer Vision*, 2013, pp. 2048–2055.
- [17] B. Drost, M. Ulrich, N. Navab, and S. Ilic, "Model globally, match locally: Efficient and robust 3d object recognition," in *2010 IEEE Computer Society Conference on Computer Vision and Pattern Recognition*, 2010, pp. 998–1005.
- [18] S. Hinterstoisser, V. Lepetit, N. Rajkumar, and K. Konolige, "Going further with point pair features," in *Computer Vision – ECCV 2016*, B. Leibe, J. Matas, N. Sebe, and M. Welling, Eds., Cham: Springer International Publishing, 2016, pp. 834–848.
- [19] M. Schwarz, H. Schulz, and S. Behnke, "Rgb-d object recognition and pose estimation based on pre-trained convolutional neural network features," in *2015 IEEE International Conference on Robotics and Automation (ICRA)*, 2015, pp. 1329–1335.
- [20] E. Brachmann, A. Krull, F. Michel, S. Gumhold, J. Shotton, and C. Rother, "Learning 6d object pose estimation using 3d object coordinates," in *Computer Vision – ECCV 2014*, D. Fleet, T. Pajdla, B. Schiele, and T. Tuytelaars, Eds., Cham: Springer International Publishing, 2014, pp. 536–551.
- [21] A. Krull, E. Brachmann, F. Michel, M. Yang, S. Gumhold, and C. Rother, "Learning analysis-by-synthesis for 6d pose estimation in rgb-d images," English, in *Computer Vision (ICCV), 2015 IEEE International Conference on*. Dec. 2015, pp. 954–962.
- [22] F. Michel, A. Kirillov, E. Brachmann, A. Krull, S. Gumhold, B. Savchynskyy, and C. Rother, "Global hypothesis generation for 6d object pose estimation," *2017 IEEE Conference on Computer Vision and Pattern Recognition (CVPR)*, pp. 115–124, 2017.
- [23] S. Kumra and C. Kanan, "Robotic grasp detection using deep convolutional neural networks," in *2017 IEEE/RSJ International Conference on Intelligent Robots and Systems (IROS)*, Sep. 2017, pp. 769–776.
- [24] Pedram Azad, Tamim Asfour, and R. Dillmann, "Stereo-based 6d object localization for grasping with humanoid robot systems," in *2007 IEEE/RSJ International Conference on Intelligent Robots and Systems*, San Diego, CA, USA: IEEE, Oct. 2007, pp. 919–924.
- [25] A. Morales, T. Asfour, P. Azad, S. Knoop, and R. Dillmann, "Integrated grasp planning and visual object localization for a humanoid robot with five-fingered hands," in *2006 IEEE/RSJ International Conference on Intelligent Robots and Systems*, Beijing, China: IEEE, Oct. 2006, pp. 5663–5668.
- [26] K. Huebner, K. Welke, M. Przybylski, N. Vahrenkamp, T. Asfour, D. Kragic, and R. Dillmann, "Grasping known objects with humanoid robots: A box-based approach," in *2009 International Conference on Advanced Robotics*, 2009, pp. 1–6.
- [27] M. Ciocarlie, K. Hsiao, E. G. Jones, S. Chitta, R. B. Rusu, and I. A. Şucan, "Towards reliable grasping and manipulation in household environments," in *Experimental Robotics: The 12th International Symposium on Experimental Robotics*, O. Khatib, V. Kumar, and G. Sukhatme, Eds. Berlin, Heidelberg: Springer Berlin Heidelberg, 2014, pp. 241–252.
- [28] A. Collet, M. Martinez, and S. S. Srinivasa, "The moped framework: Object recognition and pose estimation for manipulation," *I. J. Robotics Res.*, vol. 30, no. 10, pp. 1284–1306, 2011.
- [29] I. Lenz, H. Lee, and A. Saxena, "Deep learning for detecting robotic grasps," *The International Journal of Robotics Research*, vol. 34, no. 4-5, pp. 705–724, 2015.
- [30] K. Simonyan and A. Zisserman, "Very deep convolutional networks for large-scale image recognition," *CoRR*, vol. abs/1409.1556, 2014.

- [31] K. He, X. Zhang, S. Ren, and J. Sun, "Deep residual learning for image recognition," *2016 IEEE Conference on Computer Vision and Pattern Recognition (CVPR)*, pp. 770–778, 2016.
- [32] Y. Wu *et al.*, *Tensorpack*, <https://github.com/tensorpack/>, 2016.
- [33] J. Mahler, J. Liang, S. Niyaz, M. Laskey, R. Doan, X. Liu, J. A. Ojea, and K. Goldberg, "Dex-net 2.0: Deep learning to plan robust grasps with synthetic point clouds and analytic grasp metrics," Mar. 27, 2017.
- [34] H. Caesar, J. Uijlings, and V. Ferrari, "Coco-stuff: Thing and stuff classes in context," in *Computer vision and pattern recognition (CVPR), 2018 IEEE conference on*, IEEE, 2018.
- [35] B. Calli, A. Singh, J. Bruce, A. Walsman, K. Konolige, S. Srinivasa, P. Abbeel, and A. M. Dollar, "Yale-cmu-berkeley dataset for robotic manipulation research," *The International Journal of Robotics Research*, vol. 36, no. 3, pp. 261–268, 2017.